The Astrophysical Journal, 850:28 (12pp), 2017 November 20 https://doi.org/10.3847/1538-4357/aa93d9

Is the Gas-phase OH+H_2CO Reaction a Source of HCO in Interstellar Cold Dark Clouds? A Kinetic, Dynamic, and Modeling Study

A. J. Ocaña[1], E. Jiménez[1,2], B. Ballesteros[1,2], A. Canosa[3], M. Antiñolo[2], J. Albaladejo[1,2], M. Agúndez[4], J. Cernicharo[4], A. Zanchet[5], P. del Mazo[5], O. Roncero[5], and A. Aguado[6]

[1] Departamento de Química Física, Facultad de Ciencias y Tecnologías Químicas, Universidad de Castilla-La Mancha, Avda. Camilo José Cela 1B, E-13071, Ciudad Real, Spain; elena.jimenez@uclm.es
[2] Instituto de Investigación en Combustión y Contaminación Atmosférica, Universidad de Castilla-La Mancha, Camino de Moledores s/n, E-13071, Ciudad Real, Spain
[3] Institut de Physique de Rennes, UMR 6251 CNRS-Université de Rennes 1, Campus de Beaulieu, Bât 11C, 263 Av. Général Leclerc, F-35042, Rennes, France
[4] Instituto de Ciencia de Materiales de Madrid, Consejo Superior de Investigaciones Científicas, C/Sor Juana Inés de la Cruz, 3, E-28049, Cantoblanco, Madrid, Spain; jose.cernicharo@csic.es
[5] Instituto de Física Fundamental, CSIC, C/Serrano, 123, E-28006, Madrid, Spain; octavio.roncero@csic.es
[6] Departamento de Química Física Aplicada (UAM), Unidad Asociada IFF-CSIC, Facultad de Ciencias C-XIV, Universidad Autónoma de Madrid, E-28049, Madrid, Spain

Received 2017 July 24; revised 2017 October 4; accepted 2017 October 12; published 2017 November 14

Abstract

The chemical kinetics of neutral–neutral gas-phase reactions at ultralow temperatures is a fascinating research subject with important implications on the chemistry of complex organic molecules in the interstellar medium ($T \sim$ 10–100 K). Scarce kinetic information is currently available for these kinds of reactions at $T < 200$ K. In this work, we use the Cinétique de Réaction en Ecoulement Supersonique Uniforme (CRESU; Reaction Kinetics in a Uniform Supersonic Flow) technique to measure for the first time the rate coefficients (k) of the gas-phase OH+H_2CO reaction between 22 and 107 K. The k values greatly increase from 2.1×10^{-11} cm^3 s^{-1} at 107 K to 1.2×10^{-10} cm^3 s^{-1} at 22 K. This is also confirmed by quasi-classical trajectories (QCT) at collision energies down to 0.1 meV performed using a new full dimension and ab initio potential energy surface that generates highly accurate potential and includes long-range dipole–dipole interactions. QCT calculations indicate that at low temperatures HCO is the exclusive product for the OH+H_2CO reaction. In order to revisit the chemistry of HCO in cold dense clouds, k is reasonably extrapolated from the experimental results at 10 K (2.6×10^{-10} cm^3 s^{-1}). The modeled abundances of HCO are in agreement with the observations in cold dark clouds for an evolving time of 10^5–10^6 yr. The different sources of production of HCO are presented and the uncertainties in the chemical networks are discussed. The present reaction is shown to account for a few percent of the total HCO production rate. This reaction can be expected to be a competitive process in the chemistry of prestellar cores. Extensions to photodissociation regions and diffuse cloud environments are also addressed.

Key words: astrochemistry – ISM: abundances – ISM: clouds – ISM: molecules – molecular processes

1. Introduction

Chemistry in dense interstellar molecular clouds occurs typically at 10 K, a low temperature that can be considered to be at the high edge of ultracold chemistry. The formation of complex organic molecules (COMs) in space is a subject of great interest nowadays since these simple molecules are considered to be precursors of biological molecules, and it is important to determine their origin and evolution from dense clouds to protoplanetary disks. Most gas-phase neutral–neutral reactions forming these molecules have barriers and thus require an activation energy that is not available at temperatures of 10 K. Thus, these COMs have been long assumed to be formed onto interstellar ices and then released to the gas phase (Garrod & Herbst 2006; Garrod et al. 2008).

Formaldehyde (H_2CO) was the first organic polyatomic molecule observed in the interstellar medium (ISM) by Snyder et al. (1969). Since then, it has been detected in a variety of astrophysical environments with different temperature and density conditions, such as diffuse clouds (Liszt et al. 2006), starless cores (Bacmann et al. 2003), protostellar envelopes (Maret et al. 2004), and dense photodissociation regions (PDRs; e.g., Leurini et al. 2010; Guzmán et al. 2011). On cold prestellar cores, the observations of H_2CO led to relative abundances $X_{H_2CO}(=N_{H_2CO}/N_{H_2})$ in the range (0.5–9) $\times 10^{-10}$ (Bacmann et al. 2003), while in the Horsehead Nebula PDR, $X_{H_2CO} \sim$ (2–3) $\times 10^{-10}$ (Guzmán et al. 2011). Currently, the abundances of H_2CO modeled by considering pure gas-phase chemistry are well interpreted for dense cores, while in PDRs the inclusion of surface chemistry and the subsequent photodesorption is needed (Guzmán et al. 2011). Guzmán et al. showed that the destruction processes of H_2CO in the Horsehead PDR are dominated by photodissociation, while in the dense core they are controlled by reactions with ions (Guzmán et al. 2011). In cold molecular clouds and prestellar cores, where photodissociation is less important, the reaction of H_2CO with radical species, such as hydroxyl (OH) radicals, could play a significant role in the removal of formaldehyde and the formation of formyl (HCO) radicals in the gas phase via the exothermic reaction (Equation (1)):

$$H_2CO + OH \rightarrow HCO + H_2O \quad \Delta H_{298} = -127 \text{ kJ mol}^{-1}. \tag{1a}$$

Other thermodynamically accessible channels are

$$H_2CO + OH \rightarrow HC(O)OH + H \quad \Delta H_{298} = -89 \text{ kJ mol}^{-1}, \tag{1b}$$

Table 1
Observed Abundances of HCO (Relative to H_2) and H_2CO (Relative to HCO) in Cold Dark Clouds

Source	N_{HCO}/N_{H_2}	N_{H_2CO}/N_{HCO}	References
B1-b	1.8×10^{-11}	22	Cernicharo et al. (2012); Marcelino et al. (2005)
Lupus-1A	1.7×10^{-10}	⋯	Agúndez et al. (2015)
L483	9.0×10^{-11}	19	Agúndez et al. (2015); Tafalla et al. (2000)
L1495B	5.6×10^{-11}	⋯	Agúndez et al. (2015)
L1521F	1.3×10^{-11}	⋯	Agúndez et al. (2015)
Serpens South 1a	8.0×10^{-11}	⋯	Agúndez et al. (2015)
L1389	2.0×10^{-11}	⋯	Agúndez et al. (2015)
L1172	1.1×10^{-10}	⋯	Agúndez et al. (2015)
L1251A	1.2×10^{-10}	⋯	Agúndez et al. (2015)
L1512	8.1×10^{-11}	17	Agúndez et al. (2015); Young et al. (2004)
L1689B	9.3×10^{-11}	10	Bacmann et al. (2003); Bacmann & Faure (2016)
L429	2.1×10^{-11}	9	Bacmann et al. (2003); Bacmann & Faure (2016)
L1709A	3.9×10^{-11}	10	Bacmann et al. (2003); Bacmann & Faure (2016)
L1517B	⋯	7	Bacmann & Faure (2016)

$$H_2CO + OH \rightarrow CO + H_2O + H \quad \Delta H_{298} = -63 \text{ kJ mol}^{-1}. \tag{1c}$$

Sivakumaran et al. (2003) measured the yield of H atoms from reactions 1(b) and 1(c) to be very low (<4%) at room temperature, implying that HCO formation is the major reaction pathway at this temperature. Although no experimental evidence for the formation of HC(O)OH has been reported, D'Anna et al. (2003) concluded that the addition pathway would be insignificant even at high temperatures, because the barrier for the OH-addition channel 1(b) was calculated to be 33.6 kJ mol^{-1} above that of the H-abstraction reaction. In addition, its pre-exponential factor was found to be 8 times smaller than that for reaction 1(a). Channel 1(c) is a high T channel and most likely from "hot" HCO from channel 1(a), so it is unlikely as T is lowered. Anticipating what will be described further in the paper, in the present work it has been calculated that channel 1(a) is the main reaction pathway at the investigated temperatures (see Section 3). Channel 1(c) is considered within 1(a) since it corresponds to very excited HCO, which fragmentizes. This channel has been quantified to be less than 3% of the total reaction probability. Channel 1(b) has a higher saddle point and can be disregarded at T below room temperature.

HCO is an interesting radical in astrochemistry because it is an important candidate precursor for the formation of O-bearing COMs and prebiotic molecules. For example, it is assumed to be at the onset of the formation of glycolaldehyde, CH_2OHCHO, upon ice surfaces via HCO dimerization followed by successive hydrogenations (Woods et al. 2013). It is also a tracer of regions where an active photochemistry induced by far-ultraviolet radiation prevails (Gerin et al. 2009). Astronomical observations indicate that HCO is a widespread radical in cold dark clouds (Jiménez-Serra et al. 2004; Cernicharo et al. 2012; Agúndez et al. 2015; Bacmann & Faure 2016), where it is present with fractional abundances relative to H_2 of $(1.3–17) \times 10^{-11}$ (see Table 1), while at the edges of molecular clouds, where the gas is exposed to ultraviolet radiation, its abundance is greatly enhanced (Gerin et al. 2009). In the Horsehead Nebula, the abundance of HCO relative to H_2 varies from below 7×10^{-11} in the dense shielded core to $\sim(1–2) \times 10^{-9}$ in the PDR (Gerin et al. 2009; Guzmán et al. 2011). The source of HCO radicals, however, remains unclear (see, e.g., Gerin et al. 2009; Agúndez et al. 2015; Bacmann & Faure 2016), with various potentially important formation routes, both on the surfaces of dust grains and in the gas phase. In prestellar cores, the role of the reaction between OH and H_2CO in the formation of HCO has been recently investigated (Bacmann & Faure 2016). These authors modeled the HCO abundance employing a rate coefficient for reaction 1(a) of 10^{-11} cm^3 s^{-1}, which was obtained from experimental literature measurements at 230 K, since no measurements at lower temperatures were available. In both PDRs and cold dark clouds, the reaction between atomic oxygen and CH_2 radicals has been invoked as one potential major route to HCO (Gerin et al. 2009; Agúndez et al. 2015),

$$O + CH_2 \rightarrow HCO + H. \tag{2}$$

Other important synthetic pathways to HCO are reactions involving ions, such as the reaction of O and $C_2H_4^+$ (reaction (3)) or the dissociative recombination of H_2COH^+ (Agúndez et al. 2015; Bacmann & Faure 2016):

$$O + C_2H_4^+ \rightarrow HCO + CH_3^+, \tag{3}$$

$$H_2COH^+ + e^- \rightarrow HCO + H + H. \tag{4}$$

The kinetic behavior of these reactions, i.e., their rate coefficients and products distribution, is not fully known at low temperatures, making it difficult to precisely evaluate their role in the formation of HCO.

In astrochemical models, the T-dependence of k is commonly described by a three-parameter expression:

$$k(T) = \alpha(T/300 \text{ K})^{\beta} \exp(-\gamma/T) \text{cm}^3 \text{ s}^{-1}. \tag{5}$$

Recent experimental work at temperatures in the range 23–140 K have demonstrated that the rate coefficient for the reaction of methanol with the OH radical increases enormously at temperatures below 200 K (Shannon et al. 2013; Antiñolo et al. 2016). Similar results have also been found for other OH reactions with COMs, such as acetone, methyl ethyl ketone or ethanol (Shannon et al. 2010, 2013), and methyl formate (Jiménez et al. 2016). The surprise for the scientific community is that all these reactions present a reaction barrier, and, according to the usual transition state theory (TST), the reaction rate coefficient should decrease when lowering the temperature. These results have enormous implications because they can

open new chemical routes in the ISM networks. From a theoretical point of view, it is important to understand the reaction mechanism: how well do we understand the quantum effects? The observed increase in the OH reactivity at ultralow temperatures has been theoretically interpreted for methanol by the formation of a long-lived hydrogen-bonded complex that can undergo quantum-mechanical tunneling to form products (Shannon et al. 2013). Even though the temperature dependence of the calculated rate coefficients using the Master Equation Solver for Multi Energy-well Reactions (MESMER) equation is qualitatively correct, the values of k do not match the experimental ones. Thus, tunneling corrections have been included in order to reproduce the experimental rate coefficients. But some controversy remains concerning the possible presence of methanol dimers that may affect the experimental conclusions for the rate coefficient determination for the OH + CH_3OH reaction (Siebrand et al. 2016). Further theoretical and experimental investigations are presently in progress involving our laboratories and our colleagues in Leeds.

For the title reaction, several studies of the stationary ab initio points have been performed using different levels of theory (Alvarez-Idaboy et al. 2001; D'anna et al. 2003; Xu et al. 2006; Zhao et al. 2007; Zhang et al. 2014; Akbar Ali & Barker 2015) showing a small activation barrier that is either negative or positive (-1 to $+$ 2 kcal mol^{-1}) for channel 1(a). The reaction rate coefficients, $k_1(T)$, were obtained using TST (Alvarez-Idaboy et al. 2001; D'anna et al. 2003; Xu et al. 2006; Zhao et al. 2007; Zhang et al. 2014; Akbar Ali & Barker 2015), leading to satisfactory results in the temperature range studied ($T > 200$ K) when tunneling is added. At the lower temperatures studied in this work, it is necessary to perform precise dynamical calculations on the reactive collision, with the proper description of long-range interactions and energetics, especially the stationary points of the potential energy surface (PES). Ab initio molecular dynamics methods are therefore prohibitive, not only because of the computing time of a single point but also because the number of points on each individual trajectory is very high. Thus, an analytic fit is required to study the collision dynamics under these conditions.

For the astrochemical community, it is crucial to determine the gas-phase rate coefficients at low temperatures for many reactions that were until now neglected but may have an important impact in understanding the formation of COMs in space. Up to now, kinetic parameters for the OH+H_2CO reaction have been reported between 202 and 1670 K, temperatures of interest in the fields of atmospheric chemistry and combustion chemistry (Atkinson et al. 2006 and references therein). Compilation of these studies shows that the rate coefficient $k_1(T)$ has a positive temperature dependence in the 300–1670 K range. More interestingly, a minimum in the rate coefficient seems to be reached between 200 and 300 K, as in the reactions of OH with aforementioned COMs.

In the present work, we have gathered unique abilities of four research groups in order to explore experimentally and theoretically the kinetics and dynamics of the gas-phase OH + H_2CO reaction at very low temperature and analyze its impact on interstellar chemistry. To match these objectives, we have (i) measured the rate coefficient at temperatures of the ISM (22–107 K) using the CRESU technique; (ii) developed detailed calculations to gain more knowledge of the dynamical behavior, going beyond the TSTs or analogous, and determined the reactive cross section between 0.1 and 1000 meV using a high-quality PES to estimate the rate coefficient in the temperature range of the experiment; and (iii) evaluated the impact of the obtained temperature dependence of $k_1(T)$ on the formation of HCO in cold interstellar clouds.

The present work constitutes the very first investigation of the kinetics and dynamics of H_2CO with a radical (here OH) at temperatures relevant to cold objects of the ISM.

2. Methods

2.1. Experiments

The CRESU technique and the experimental setup employed have been previously described elsewhere (Antiñolo et al. 2016; Jiménez et al. 2015, 2016), and only a brief overview will be given below. A set of five Laval nozzles were used to get the jet temperatures between 22 and 107 K, and characterization of the obtained flows was discussed elsewhere (Canosa et al. 2016). The adiabatic gas expansion through the Laval nozzle from the reservoir to the reaction chamber provokes the cooling of the gas and forms a uniform jet in temperature and total gas density over several tens of cm, i.e., over several hundreds of μs hydrodynamic time, $t_{\rm hydro}$ (Table 3). OH radicals were generated in the gas jet by pulsed laser photolysis of gaseous H_2O_2 at 248 nm. The time evolution of OH radicals in the presence and absence of H_2CO was monitored by laser-induced fluorescence (LIF) ca. 310 nm, which was collected by a filtered photomultiplier tube. The excitation wavelength (282 nm) was delivered from a frequency-doubled dye laser pumped by the second harmonic of an Nd-YAG laser. The analysis of the exponential decays yields the pseudo–first-order rate coefficient, k', which is linearly related to [H_2CO] concentration under pseudo–first-order conditions (Appendix Figure 8). Varying the mass flow rate of a diluted mixture containing a well-known quantity of H_2CO and maintaining the OH-precursor concentration constant, $k_1(T)$ was obtained from the slope of the plot of k' (or k'–k_0) versus [H_2CO] (Appendix).

2.2. Quasi-classical Trajectory (QCT) Simulations

A full-dimensional analytical PES has been developed to treat the reaction dynamics at temperatures below 100 K, as described in a recent publication (Zanchet et al. 2017). The intrinsic reaction coordinate (IRC) diagram in Figure 1 shows the quality of the analytical fit and describes the energy diagram of the reaction.

QCT calculations have been performed using an extension of the code miQCT applied to N atoms (Dorta-Urra et al. 2015). The Hamilton equations are integrated using a step-adaptive Adams–Bashforth–Moulton predictor-corrector method (Shampine & Gordon 1975), using the Cartesian coordinates of the position vectors of all atoms. The total integral cross section, $\sigma_{\rm vj}(E)$, is calculated according to the following equation (Karplus et al. 1965),

$$\sigma_{\rm vj}(E) = \pi b_{\rm max}^2 P_{\rm r}(E), \quad (6)$$

where $b_{\rm max}$ is the maximum impact parameter corresponding to the maximum distance at which trajectories are efficiently deviated to form products and $P_{\rm r}(E)$ is the reaction probability given by

$$P_{\rm r}(E) = N_{\rm r}(E)/N_{\rm tot}(E), \quad (7)$$

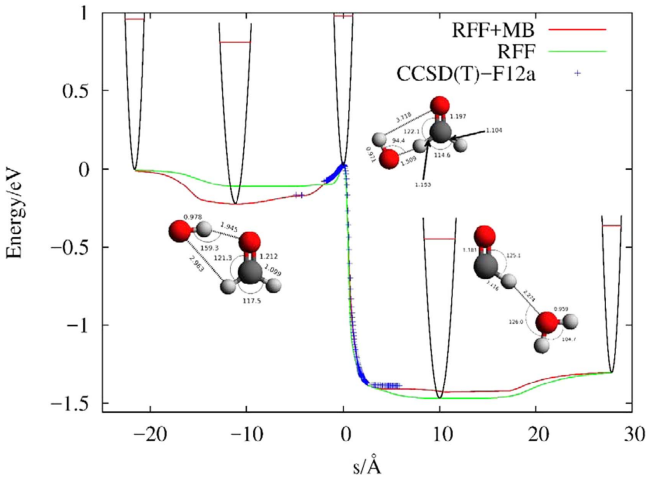

Figure 1. IRC diagram for the ab initio, RFF, and RFF+MB PESs. The geometries of reactants and product wells and the saddle point are also displayed.

where $N_{\rm tot}(E)$ is the maximum number of trajectories at collision energy E with $b < b_{\rm max}$, while $N_{\rm r}(E)$ is the number of reactive trajectories leading to products.

A Monte Carlo sampling of initial conditions is done for each reagent independently (OH and H_2CO). To include the zero-point energy (ZPE), an adiabatic switching method is performed (Grozdanov & Sovolev 1982; Johnson 1987; Qu & Bowman 2016). In this method, a random selection of initial conditions is done according to analytical normal modes, and then the harmonic potential is adiabatically switched to the real one. Since the energy spreading is rather high, we select a particular trajectory with the closest energy to the anharmonic ground state eigenvalue of each fragment, which is propagated for 100,000 steps. In this case, OH and H_2CO are initially set at zero angular momentum by using the method of Nyman and coworkers (Nyman et al. 1990). Once the internal vibrational distribution is set, the relative orientation of the two fragments is randomly selected. The impact parameter is randomly selected up to a maximum distance $b^0_{\rm max}$, at which trajectories are efficiently deviated. This maximum value is given by the capture model (Levine & Bernstein 2001):

$$b^0_{\rm max} = 3^{1/2}(A/2E)^{1/3}. \quad (8)$$

The initial distance between the two reagents is set to 120 au. These long distances are required for the low energies considered here.

In the present system, the long-range interaction between the permanent dipole moments (d_X, X = OH and H_2CO) varies as:

$$V(R \to \infty) = \frac{-A}{R^3} \quad (9)$$

with $A = 4\ d_{\rm OH}\ d_{\rm H_2CO}$.

Two different strategies are followed to analyze the collision dynamics.

(1) First, the individual cross section for H_2CO and OH in the ground vibrational and rotational states is calculated in the microcanonical ensemble according to Equation (6). This is done using a grid of collision energies from 0.1 to 1000 meV. For each translational energy, 10^5 trajectories were run. Finally, the state-dependent rate, $k_{v=0,j=0}(T)$, is obtained by numerical integration over a Boltzmann distribution. The final rate coefficient $k^{\rm e}_{v=0,j=0}(T)$ is obtained by multiplying this $k_{v=0,j=0}(T)$ by the electronic partition function, $q_{\rm e}$, described in Section 3.

(2) Second, the thermal rate coefficients, $k(T)$, are obtained from Equation (10) by running 10^6 trajectories for each temperature in the macrocanonical ensemble, defining initial conditions for thermal rotational distributions of the two reagents,

$$k(T) = q_e\left(\frac{8kT}{\pi\mu}\right)^{\frac{1}{2}}\pi b^2_{\rm max}\,P_r(T), \quad (10)$$

where μ is the reduced mass of the OH + H_2CO system.

2.3. Chemical ISM Model

To evaluate the hypothesis that H_2CO could be a precursor of HCO radicals in cold interstellar clouds, we have run a chemical model of a cold dark cloud in which we adopt typical parameters, i.e., a kinetic temperature of 10 K, a volume density of H nuclei of 2×10^4 cm^{-3}, a visual extinction of 30 mag, a cosmic-ray ionization rate of H_2 of 1.3×10^{-17} s^{-1}, and the so-called "low-metal" elemental abundances (Agúndez & Wakelam 2013). We have run models using two chemical networks to have an idea of the robustness of the results. Concretely, we have used the network kida.uva.2014 from the KIDA (KInetic Database for Astrochemistry) database (Wakelam et al. 2015) and the rate 2012 network from the UMIST (University of Manchester Institute of Science and Technology) database (McElroy et al. 2013). In both chemical networks, we have implemented the reaction H_2CO + OH→ HCO + H_2O with the extrapolated rate coefficient at 10 K obtained in this work (see Section 3.1).

3. Results and Discussion

3.1. Gas-phase Kinetics of the OH+H_2CO Reaction between 22 and 107 K

The measured rate coefficients $k_1(T)$ have been compiled in Table 2. They have been determined at ca. 22 K using three different Laval nozzles with total He densities ranging from 3.37×10^{16} to 1.67×10^{17} cm^{-3}. At ca. 45 K, two Laval nozzles were employed for different gas densities, 6.90×10^{15} and 1.02×10^{17} cm^{-3}(N_2 and N_2/He, respectively). All physical conditions for all Laval nozzles employed are listed in Table 3. In Table 2, $k_1(T = 22$ K) and $k_1(T = 45$ K) are presented at each gas density. As can be seen, no pressure dependence of $k_1(T = 22$ K) was observed in the investigated gas-density range, implying that reaction (1) at these temperatures is either a bimolecular reaction or a three-body process already in the high-pressure limit at the lowest gas density. At 45 K, a decrease of 27% is observed in k_1 when the gas density is varied by more than one order of magnitude. Within the experimental uncertainties, this decrease is not expected to be originated by a pressure effect. Such an effect on $k_1(T)$ should be more noticeable at even higher temperatures for which the rate coefficient is lower and then separates even more from the high-pressure limit of a falloff curve. In other words, the high-pressure limit would be reached at higher total pressures. At the highest temperatures investigated in this work (107 K), it can be seen that the rate coefficient is similar to that at 89 K (see Table 2), whereas the total density (1.8×10^{17} cm^{-3}) is 3.6 times higher. If the process was thermolecular, one

Table 2
Rate Coefficients for the Gas-phase Reaction between OH Radical and H_2CO as a Function of Gas Density and Temperature[a]

T (K)	n (10^{16} cm^{-3})	$k_1(T)$[b] (10^{-11} cm^3 s^{-1})	$k_1(T)$ (10^{-11} cm^3 s^{-1})
21.1 ± 0.6	3.37 ± 0.15	9.1 ± 1.1	10.1 ± 1.0[c]
	⋯	10.0 ± 1.1	⋯
	⋯	12.9 ± 1.6	⋯
21.7 ± 1.4	16.65 ± 1.61	12.3 ± 1.3	12.3 ± 1.2[c]
	⋯	12.1 ± 1.6	⋯
22.5 ± 0.7	7.43 ± 0.32	11.8 ± 1.5	12.0 ± 1.2[c]
	⋯	12.0 ± 1.3	⋯
36.2 ± 1.2	17.73 ± 0.86	⋯	8.62 ± 0.86
45.6 ± 1.4	10.19 ± 0.52	6.59 ± 0.69	6.09 ± 0.76[c]
	⋯	5.74 ± 0.66	⋯
	⋯	5.50 ± 0.62	⋯
	⋯	6.09 ± 0.64	⋯
45.5 ± 2.0	0.69 ± 0.08	⋯	4.44 ± 0.45
51.6 ± 1.7	4.17 ± 0.35	⋯	4.17 ± 0.43
55.4 ± 1.4	3.02 ± 0.23	⋯	4.14 ± 0.42
78.2 ± 1.0	2.45 ± 0.08	⋯	2.77 ± 0.29
89.5 ± 0.6	18.24 ± 0.33	⋯	2.39 ± 0.25
107.0 ± 0.5	4.90 ± 0.06	⋯	2.15 ± 0.22

Notes.
[a] Uncertainties in T and n are the standard deviation (only statistical).
[b] Stated uncertainties are the combination of the statistical and systematic (±10%) errors.
[c] Averaged value of different experiments.

should expect that k_1 would increase with gas density and when the temperature is lowered. Hence, we should have found a significantly higher value at 89 K than at 107 K, while it was found, within the experimental uncertainties, $k_1(89\ \mathrm{K}) \cong k_1(107\ \mathrm{K})$. For all these reasons, it can be argued that reaction (1) is essentially bimolecular in the temperature range of the present work. As shown in Table 2, an increase in $k_1(T)$ is observed when lowering T.

When combining our data with those reported by Sivakumaran et al. (2003) at $T < 300$ K, the best fit is

$$k_1(T = 22\text{–}300\mathrm{K}) = (7.73 \pm 1.82) \times 10^{-12} \times (T/300\ \mathrm{K})^{-(1.03\pm0.09)}\ \mathrm{cm^3\ s^{-1}}, \quad (11)$$

where the uncertainties are $\pm 2\sigma$. The relative difference of the calculated $k_1(T)$ from Equation (11) with respect to the experimental values in the range 22–107 K varies from 4% to 21%. In Figure 9, the confidence-interval bands of the fit are depicted at a 95% level of confidence in addition to the experimental data and the abovementioned fit. The $k_1(T)$ values in the 200–300 K range are predicted by Equation (11) within an uncertainty of 1%–5% for most of the available measurements.

As can be seen in Figure 2, when comparing our results with all of the previous kinetic studies on the OH + H_2CO reaction between 200 and 1500 K, a U-shaped curvature is observed in the trend of $k_1(T)$, with a minimum value around 300 K. The three-parameter expression recently proposed by Wang et al. (2015), which combines their high-temperature data with those at lower temperatures from Sivakumaran et al. (2003), is shown by a blue solid line in Figure 2. This expression represents perfectly experimental data for $T > 200$ K (within 6%–15%) but fails to predict $k_1(T)$ at $T < 120$ K (difference >50%). For example, the predicted $k_1(T = 107\ \mathrm{K})$ is almost twice the experimental value. Therefore, we recommend using our expression for $k_1(T)$ below 250 K and Wang's formula above. Our expression has been derived in the range 22 K $< T <$ 250 K. Even though extrapolation can be risky, Equation (11) can be used to obtain an estimation of the rate coefficient at 10 K needed for the modeling of HCO and H_2CO abundances in cold interstellar clouds. This leads to a value of $(2.60 \pm 0.60) \times 10^{-10}$ cm^3 s^{-1}.

3.2. Dynamics of the OH + H_2CO Reaction

The experimental determination of the reaction rate coefficient is done through the disappearance of the OH. One way to check if the measured disappearance of OH corresponds to the formation of the HCO product is to perform complete dynamical simulations of the $H_2CO + OH \rightarrow HCO + H_2O$ reactive collisions. This reaction presents a low barrier of 27 meV, with a ZPE of the order of 1 eV (see Figure 1), in agreement with previous studies. If pure TST is applied and the reaction coordinate is separated from the orthogonal vibrational modes, the reaction would not happen for collision energies below 27 meV (approximately 300 K), and the rates would tend to zero when decreasing temperature, in opposition to the behavior of the experimental results. One way to overcome this difficulty is to introduce tunneling in the TST model, giving rise to different approaches based essentially in the anharmonicity of the potential at the saddle point. These approaches are approximate, and the purpose of this work is to carry out full-dimension reaction dynamics studies that better describe the reaction mechanism at low temperatures.

QCT calculations have been done for the $H_2CO + OH \rightarrow HCO + H_2O$ reaction on the reactive force field (RFF) and the full (RFF+MB (many-body)) PESs described in Zanchet et al. (2017). These PESs were developed on purpose and properly describe the long-range interactions and all the energetics, especially the stationary points of the PES. The calculations performed in the microcanonical ensemble at fixed collision energy allow a better understanding of the reaction mechanism. The total reaction cross section, $\sigma_{v=0,j=0}(E)$, calculated for the ground rotational and vibrational state of the two reactants shows a continuous increase with decreasing collision energy for both the total RFF+MB and RFF PESs (see bottom panel of Figure 3). Clearly, the increase of σ_{vj} is associated with the increase of b_{max} (middle panel of Figure 3), while $P_r(E)$ remains nearly constant (top panel of Figure 3). The increase in the impact parameter is well described by the capture model (Levine & Bernstein 2001) using Equation (8). The agreement with the one found in the QCT simulations is nearly perfect until an energy of 100 meV, where the corresponding b_{max} is of the order of the size of the molecules. This confirms that the potential is able to capture trajectories at low energy with an increasing efficiency as collision energy decreases. This leads to trajectories that are trapped in the OH–H_2CO well for a long time, where the dynamics becomes ergodic and chaotic, as recently found in ultracold collisions (Croft & Bohn 2014).

In the top panel of Figure 3, it is shown that $P_r(E)$ changes smoothly with the collision energy and does not drop to zero even at 0.1 meV, energy well below the reaction barrier of the two PESs (of 27 meV). The difference between the reaction cross section found for the two PESs, RFF and RFF+MB, is explained by the change in the reaction probability, since the

Table 3
Summary of the Experimental Conditions in the CRESU System: Pressure (P_{res}) in the Reservoir, Pressure (P_{cham}) in the Chamber, Mach Number (M), Hydrodynamic Time (t_{hydro}), Total Gas Density (n), and Temperature of the Jet (T)

Bath Gas	P_{res} (mbar)	P_{cham} (mbar)	M	t_{hydro} (μs)	n (10^{16} cm^{-3})	T (K)
He	73.88	0.125	6.27 ± 0.10	165	3.37 ± 0.15	21.1 ± 0.6
He	337.2	0.62	6.13 ± 0.21	238	16.65 ± 1.61	21.7 ± 1.4
He	147.76	0.28	6.05 ± 0.09	320	7.43 ± 0.32	22.5 ± 0.7
He	173.32	1.10	4.65 ± 0.08	304	17.73 ± 0.86	36.2 ± 1.2
N_2	31.17	0.05	5.26 ± 0.13	760	0.69 ± 0.08	45.5 ± 2.0
N_2/He[a]	102.96	0.74	4.34 ± 0.07	312	10.19 ± 0.52	45.6 ± 1.4
N_2	136.24	0.279	4.88 ± 0.10	777	4.17 ± 0.35	51.6 ± 1.7[b]
N_2	81.49	0.216	4.66 ± 0.08	537	3.02 ± 0.23	55.4 ± 1.4[b]
N_2	28.56	0.283	3.74 ± 0.03	297	2.45 ± 0.08	78.2 ± 1.0[b]
N_2	151.59	2.37	3.40 ± 0.02	610	18.24 ± 0.33	89.5 ± 0.6
N_2	26.12	0.79	2.98 ± 0.01	382	4.9 ± 0.06	107.0 ± 0.5

Notes.
[a] 80% He and 20% N_2.
[b] Continuous mode. Uncertainties are the standard deviation.

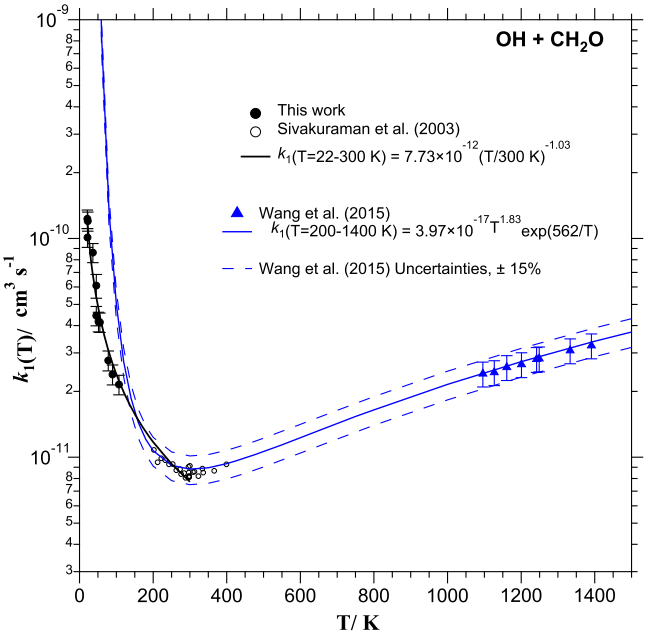

Figure 2. Temperature dependence of the rate coefficient of the OH + H_2CO reaction between 22 and 1400 K. The equation recently proposed by Wang et al. (2015) reproduces the light curvature between 200 and 400 K; however, it is not consistent with the experimental data below 200 K (see text).

impact parameter remains nearly the same for both PESs. This change of the reaction probability is attributed to the many-body term introduced in the potential to better describe the calculated ab initio points. The RFF by itself is too isotropic, facilitating access from the complex to the saddle point, giving rise to an overestimation of the reaction cross section. This fact is corrected by the MB term.

The remaining point to understand is why the reaction probability is nonzero at energies below the top of the barrier. Considering the ZPE of reactants, the system has enough total energy to overcome this barrier. If the reactants' ZPE remains in the coordinates orthogonal to the reaction coordinate, the reaction could not take place, since there would not be enough energy in the reaction coordinate. Clearly, this is not the case, and there must be couplings between the reaction coordinate and the remaining degrees of freedom producing an energy transfer that explains the nonzero reaction probability even at

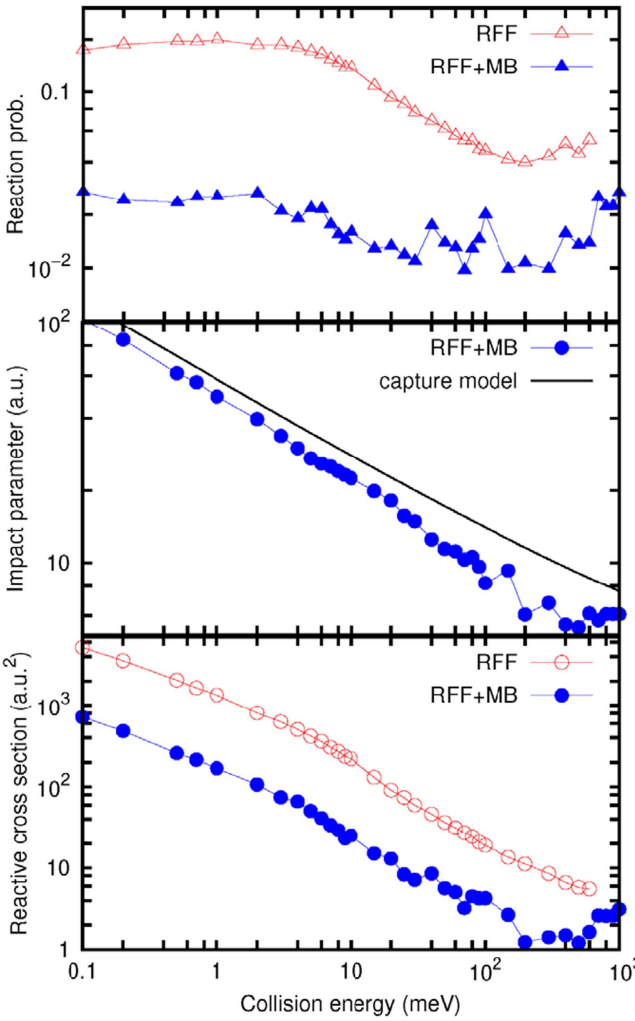

Figure 3. Top panel: reactive probabilities $P_r(E)$ as a function of collision energy. Middle panel: impact parameter b_{max} as a function of collision energy. Bottom panel: reactive cross section. All quantities have been calculated with the RFF (red) and RFF+MB (blue) PESs.

0.1 meV of collision energy. Such a situation is typical in non-intrinsic reaction coordinate (non-IRC) trajectories (Lourderaj et al. 2008), since they explore large regions of the

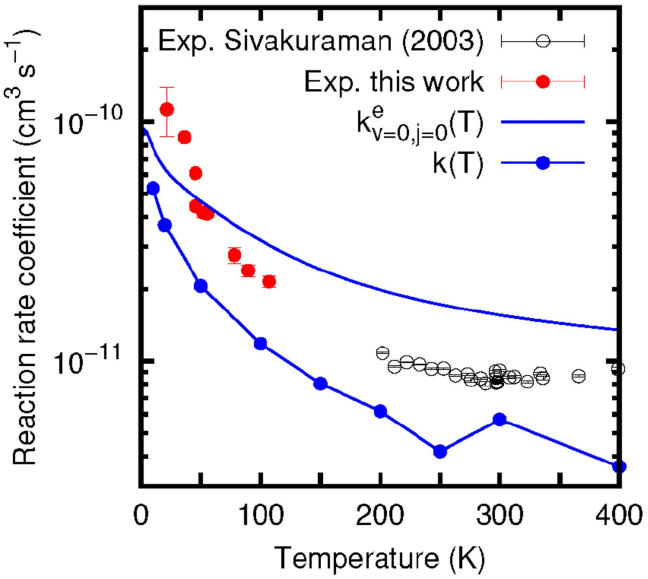

Figure 4. Simulated thermal rate coefficient, $k_1(T)$, and initial-state selected rate coefficient, $k^{e}_{v=0,j=0}(T)$, as defined in the text, compared with the experimental results in the 20 K $< T <$ 400 K temperature range.

configuration space far from the minimum energy path determined by the IRC, where the anharmonicity is larger. The concept of ZPE at the transition state is an approximation based on the separation between the reaction coordinate (in the dissociation continuum) and the orthogonal vibrations. This separation is adequate for trajectories going along the IRC, since the potential can be locally described by a parabolic separable potential. Out of this IRC the potential is no longer separable, hence the energy can be transferred among the different degrees of freedom. Moreover, the harmonic approximation made to estimate the ZPE at the saddle point is questionable, since the PES at the saddle point has a large anharmonicity that tends to reduce the ZPE.

The rate coefficient is calculated by integrating the cross section over a Boltzmann distribution. To account for the spin–orbit splitting of the OH($^2\Pi$) states into the $F_1(^2\Pi_{1/2})$ and $F_2(^2\Pi_{3/2})$ with an energy separation of 200.3 K, the rate coefficient is multiplied by the electronic partition function, $q_e = [1+\exp(-200.279/T)]^{-1}$. This term arises from the assumption that only the ground spin–orbit state reacts. The rate coefficient thus obtained only corresponds to the ground rotational states of OH and H_2CO, and it is labeled as $k^{e}_{v=0,j=0}(T)$ in Figure 4. In order to compare with the experimental data of this work, also in Figure 4, we have to consider the rotational populations of the reactants, which vary as a function of temperature. This is done by directly computing the thermal rate coefficient, $k(T)$, in the macrocanonical ensemble according to Equation (10), which is depicted in Figure 4. Clearly, the computed rate coefficient $k(T)$ is slightly lower than the experimental one, but it shows the same behavior. At $T > 50$ K, $k(T)$ is a factor of ca. 2 lower; however, the difference between theory and experiment increases somewhat when lowering the temperature. We therefore conclude that the behavior of the simulation is semiquantitatively correct, explaining the experimental results obtained in this work.

The quantitative differences may be attributed to two major factors. First, the reaction probabilities displayed in Figure 3 depend on the accuracy of the PES. Work is now in progress to improve the current PES. Second, quantum effects are expected to be important at low collision energies, while they are neglected in the present treatment. To analyze the qualitative effect of quantum dynamics, we can refer to a similar reaction, OH + F → O + HF, with a similar energy profile, for which the cross section also increases significantly at low energies (Gómez-Carrasco et al. 2004a, 2004b, 2005). In that triatomic system, exact quantum wave-packet calculations were performed, finding that the reaction cross section increases with decreasing collision energy, being always larger than the QCT cross sections. This behavior was interpreted by an indirect mechanism at low energies due to the presence of resonances in both the quantum and classical simulations. It may be concluded that the QCT approach yielded qualitatively good results but tended to lead to lower rate coefficients at low temperatures. Similar effects are expected in the H_2CO + OH reaction, and the inclusion of quantum effects may yield to a better agreement with experiments, especially at low temperatures. Quantum effects may be the reason for the increasing difference, particularly the ZPE effects. The reaction mechanism consists of two steps: the capture to form the complex and the dissociation to either reactants or products. The lifetime of this complex is determined by the number of open channels. This number in the products is already rather large, since the reaction is exothermic. Then, the crucial quantity determining the reactivity is the number of open channels in the reactants. For low temperatures, this number reduces to 1, i.e., the ground rovibrational state of the two reactants. This is so in a quantum description. However, using a QCT description, there is no quantization. Therefore, the dissociation back to reactants is somehow overestimated, and this probably explains the disagreement between simulations and experiments, especially at low temperatures.

The total rate coefficient corresponds to the rearrangement channel HCO + H_2O. It should be noted that the products end in highly excited rovibrational states. In the particular case of HCO, with a rather weak bond, it may fragment, giving H + CO. Thus, the formation of CO + H + H_2O is included in the present model. However, its proportion is rather low, varying between 2% and 4% in the entire temperature range.

3.3. Astrochemical Model

In order to evaluate the impact of the titled reaction on the abundances of HCO and H_2CO in cold dark clouds, we performed a chemical model using two different chemical networks, UMIST (McElroy et al. 2013) and KIDA (Wakelam et al. 2015), and set k_1(10 K) to 2.6×10^{-10} $cm^3\ s^{-1}$ (value from Equation (11)).

In Figure 5, we show the calculated fractional abundances of HCO and H_2CO as a function of time using the UMIST and KIDA networks. It is seen that the calculated abundance of HCO at times between 10^5 and 10^6 yr is in good agreement with the range of values derived from observations. Even though the reaction between H_2CO and OH is very fast at low temperatures, the chemical model indicates that it accounts for a few percent in the production of HCO radicals in cold dark clouds. This result is consistently obtained no matter which chemical network is adopted. According to the chemical model, the main HCO-forming routes are reactions involving atomic oxygen (reactions (2) and (3)) and the dissociative recombination of the molecular ion H_2COH^+ (reaction (4)). The relative importance of these reactions varies depending on the adopted

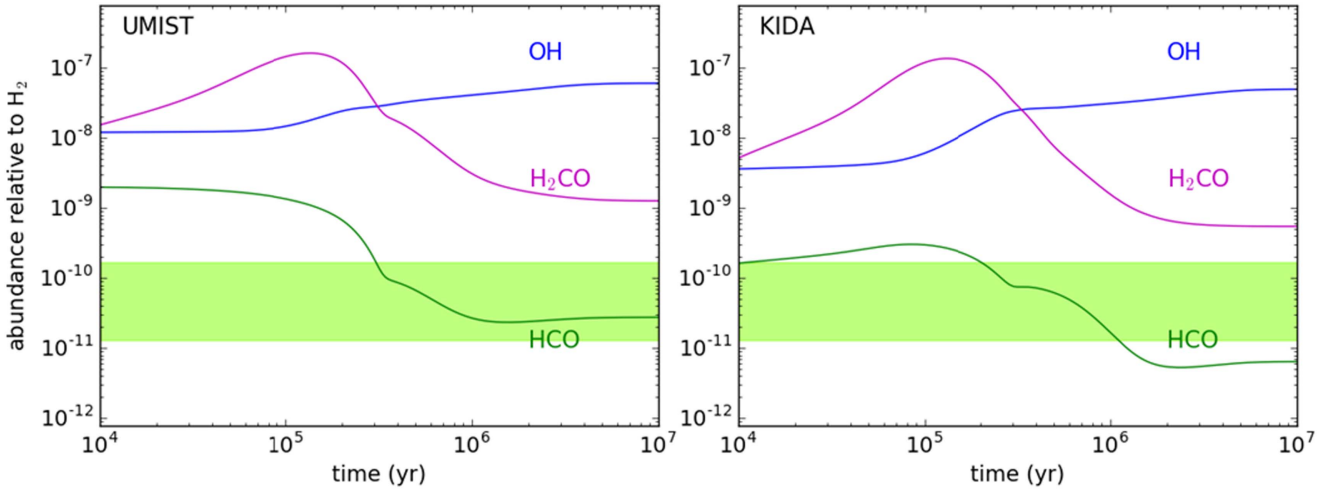

Figure 5. Calculated abundances of HCO, H_2CO, and OH in a cold dark cloud as a function of time using the UMIST (left panel) and KIDA (right panel) chemical networks. The horizontal green bands indicate the range of HCO abundances observed in cold dark clouds (see Table 1).

chemical network. This is illustrated in Figure 6, where we show the contributions of the five most important HCO-forming reactions as a function of time and compare them with the HCO production rate given by reaction (1). At times between 10^5 and 10^6 yr, reaction (2) dominates when the UMIST network is adopted, while if the KIDA network is used, the main route to HCO becomes reaction (4).

The rate coefficient of the reaction between CH_2 radicals and O atoms has been measured at room temperature (Böhland et al. 1984), although it has not been studied at low temperature and it is not clear which is the branching ratio of the channel leading to HCO. According to Böhland et al. (1984), the HCO radicals formed in the $O + CH_2$ reaction should contain enough excess energy to dissociate into CO + H. It is therefore uncertain whether reaction (2) is actually an important source of HCO radicals. The UMIST network adopts a rate coefficient of 5×10^{-11} cm^3 s^{-1} estimated in high-temperature experiments, while in the KIDA network a smaller value, 2×10^{-12} cm^3 s^{-1}, is adopted based on a discussion by Loison et al. (KIDA datasheet 281; Wakelam et al. 2015). The importance of reaction (2) strongly depends on its rate coefficient at low T. This explains the big difference between the UMIST and KIDA results shown in Figure 6. For $O + C_2H_4^+$ (reaction (3)) and $H_2COH^+ + e^-$ (reaction (4)), the kinetics is better constrained from experiments. For the first reaction, its rate coefficient has been measured to be 2.4×10^{-10} cm^3 s^{-1} at room temperature, and the branching ratio for the channel yielding HCO has been measured as 45% (Scott et al. 2000). Since the neutral reactant is nonpolar, the rate coefficient should be independent of temperature, and thus the value measured at room temperature should pertain at low temperatures as well. Therefore, the value adopted at 10 K in both networks was $k_3 = 1.08 \times 10^{-10}$ cm^3 s^{-1}.

The dissociative recombination of H_2COH^+, as with most reactions of this type, is fast at low temperatures and has been found to preserve the C–O bond in most of the collisions (Hamberg et al. 2007). The branching ratios of the channels leading to H_2CO, HCO, and CO are not known. However, they are assumed to be equal by the KIDA and UMIST networks. The values for k_4 used were 1.10×10^{-6} cm^3 s^{-1} (KIDA) and $k_4 = 3.08 \times 10^{-6}$ cm^3 s^{-1} (UMIST).

The chemistry of HCO radicals in prestellar cores was discussed by Bacmann & Faure (2016) based on simple steady-state arguments and different assumptions on the main source and sink reactions for HCO. These authors evaluated which HCO abundance would result if this radical was exclusively formed (i) by reaction (1) or (ii) by the dissociative recombination of H_2COH^+ (reaction (4)), in both cases assuming that the main sinks of HCO are reactions of proton transfer from abundant ions that can easily give a proton (e.g., HCO^+, H_3^+). They concluded that the ionic pathway scenario (reaction (4)) results in HCO abundances that agree with the values derived from observations, while the neutral–neutral reaction OH + H_2CO needs to have a rate coefficient of 4×10^{-10} cm^3 s^{-1} to produce HCO in the observed quantities. This is rather close to the value used in the present model extrapolated from our experimental results, $k_1(10\ \mathrm{K}) = 2.6 \times 10^{-10}$ cm^3 s^{-1}. According to the chemical model (see Figure 6), reaction (1) would need to be more than one order of magnitude faster than indicated by our measurements to compete with other reactions in the synthesis of HCO radicals in cold dense clouds. We stress, however, that this conclusion is based on a chemical model that is subject to significant uncertainties because the low-temperature kinetics of most of the reactions included is not precisely known, as exemplified earlier with, e.g., the $O + CH_2$ reaction.

The formyl radical is particularly abundant in PDRs, where its abundance is enhanced by two orders of magnitude with respect to cold dense clouds (Gerin et al. 2009). It is, however not clear how this radical is formed in these environments. Gerin et al. (2009) carried out a pure gas-phase model and found that HCO abundances of the order of magnitude of the observed ones can be obtained if HCO is efficiently produced in the photodissociation of H_2CO and in the reaction between CH_2 radicals and O atoms (reaction (2)). These two routes, however, lack sufficient empirical support, and it remains to be seen if alternative HCO-forming routes—as, e.g., reaction (1)—would need to be invoked to explain the relatively large abundances of HCO observed in PDRs such as the Horsehead Nebula.

In summary, despite the uncertainties in the rate coefficients and branching ratios of various reactions important for the chemistry of HCO, it seems that, in the present state of

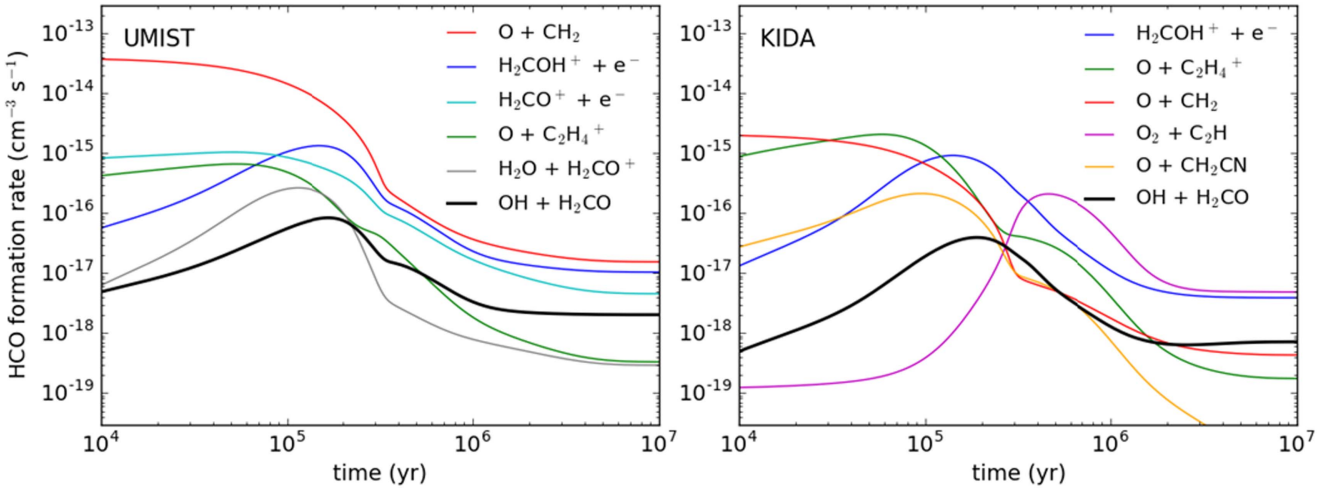

Figure 6. Contribution of the five most important reactions and reaction (1) to the formation of HCO in a cold dark cloud as a function of time, as calculated with the chemical model using UMIST (left panel) and KIDA (right panel).

knowledge and chemical uncertainties, in cold dense clouds the reaction OH + H_2CO is less efficient than alternative gas-phase routes involving O atoms and the precursor ion H_2COH^+ in the formation of HCO radicals. However, it remains to be explored whether the dramatic enhancement in the reactivity of OH and H_2CO could be responsible for the formation of HCO radicals in other relatively cold interstellar media, such as diffuse clouds and PDRs.

4. Conclusions

The rate coefficients for the H_2CO + OH reaction in the gas phase have been determined for the first time at ultralow temperatures (22–107 K) in a CRESU machine. The rate coefficient increases as the temperature decreases, although a barrier (∼300 K) is present along the reaction pathway. This behavior is also found in QCT calculations performed on a highly accurate PES especially developed for this purpose. The experimental finding is explained by two factors. First, the long-range dipole–dipole interactions are able to capture trajectories forming an OH–H_2CO long-lived complex. Second, the dynamics becomes ergodic following trajectories far apart from the minimum energy path or IRC, at which the anharmonicity of the potential is high. In this situation, the reaction coordinate is strongly coupled to the orthogonal vibrations and can exchange enough energy to overcome the barrier.

The impact of the present rate coefficients on interstellar chemistry has been addressed by exploring the potential consequences of this new data on the formation of interstellar HCO. Whereas in cold dark clouds the titled reaction was found to be a minor source of HCO with respect to alternative routes involving O atoms and dissociative recombination of H_2COH^+, it remains to be explored whether the OH + H_2CO reaction can provide a significant contribution to HCO formation in other environments, such as PDRs and diffuse clouds.

This work has been supported by the European Research Council (NANOCOSMOS, SyG-610256) and the Spanish Ministry of Science and Innovation (ASTROMOL, CSD2009-00038). Authors from UCLM acknowledge the Spanish Ministry of Economy and Competitiveness (MINECO) for supporting this work under the GASSOL project (CGL2013-43227-R). Authors from ICMM acknowledge financial support from MINECO through grants AYA2012-32032 and AYA2016-75066-C2-1-P. M. Agúndez thanks the Ramón y Cajal program of MINECO (RyC-2014-16277). M. Antiñolo would like to thank UCLM (Plan Propio de Investigación) for funding. AC thanks the French national program "Physique et Chimie du Milieu Interstellaire" (PCMI) from the Institut National des Sciences de l'Univers (INSU) and the European COST program CM1401 "Our Astrochemical History" for financial support. AZ, PM, OR, and AA acknowledge the support of MINECO for grant FIS2014-52172-C2 and the European COST program CM1401 "Our Astrochemical History." The calculations were performed at the CSIC computing centers, which are acknowledged. We thank J. R. Goicoechea for discussions on the chemistry of HCO in PDRs.

Appendix

Synthesis and Spectroscopic Quantification of Formaldehyde. H_2CO is produced off-line and under vacuum by heating paraformaldehyde (Acros Organics, 96%). The solid is placed in a glass vessel, which is connected to a blackened 10-L bulb and a rotary pump. The glass vessel is submerged in a polyethylene glycol bath while being heated up to about 60° C to degas the sample through a cold trap at 77 K. Afterward, paraformaldehyde is heated to about 100°–110° C during 1 hr. The increase of pressure in the system formed by the glass vessel and the 10-L bulb due to the formation of H_2CO is monitored by a 100 Torr pressure gauge (Ceravac CTR100N from Leybold). The heating is stopped when the pressure in the system reaches ∼100 mbar, then H_2CO is stored. A partial pressure of 10–20 mbar is taken from the 10-L bulb and further diluted up to 1000–1100 mbar of the buffer gas (N_2 or He) in another 40-L bulb to achieve the desired concentrations in the kinetic experiments before the gas expansion. The H_2CO concentrations in these gas mixtures are checked before starting the kinetic experiments and just after by UV spectroscopy using the setup described in Jiménez et al. (2005) in order to ensure that the concentration obtained by the dilution method is not affected by potential polymerization of H_2CO, which may occur in the bulb within the timescale of an experiment at a

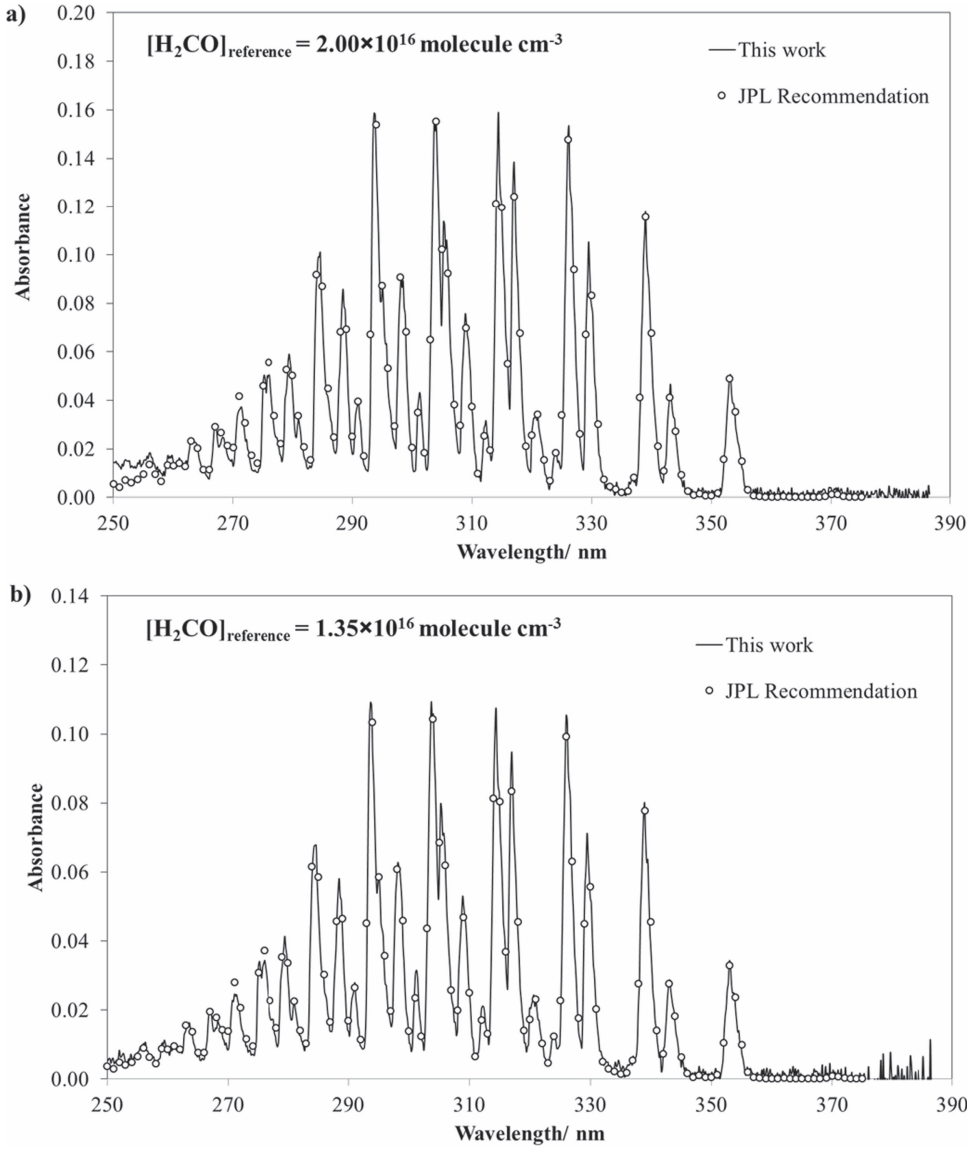

Figure 7. UV spectrum of formaldehyde recorded at two total pressures of a diluted mixture in N_2 with a mixing ratio of 7.53×10^{-3}: (a) 82.3 Torr ($\equiv 2.00 \times 10^{16}$ molecule cm^{-3}) and (b) 55 Torr ($\equiv 1.35 \times 10^{16}$ molecule cm^{-3}). Path length = 107 cm.

given temperature. In Figure 7, two examples of the UV spectrum (in base *e*) recorded between 250 and 380 nm are shown. Circles correspond to the simulated UV spectrum obtained using the absorption cross sections recommended by the JPL-NASA panel (Atkinson et al. 2004) and the concentration of formaldehyde derived from the pressure measurements. Wavelengths from JPL recommendations are in air. As can be seen, the simulated UV spectrum of formaldehyde matches (<1%) the experimental UV spectrum at the concentrations in the storage bulb at room temperature.

Kinetic analysis. The kinetic experiments are performed in pseudo–first-order conditions (i.e., $[H_2CO] \gg [OH]$ and $[H_2O_2] \gg [OH]$). In the absence of formaldehyde, OH radicals are mainly reacting with its photochemical precursor H_2O_2. Diffusion of OH radicals out of the detection zone can be neglected under these conditions. From the exponential decays of [OH], the pseudo–first-order rate coefficients, k', are obtained for different $[H_2CO]$. Here, k_0 is the measured rate coefficient in the absence of formaldehyde at the same temperature. In the experimental conditions, k' varies linearly with $[H_2CO]$ as

$$k' = k_0 + k_1(T)[H_2CO]. \quad (12)$$

The bimolecular rate coefficient for reaction (1) at a given temperature $k_1(T)$ is obtained from the slope of the k' versus $[H_2CO]$ plots. In order to compare different experiments, Equation (12) is expressed in terms of k'–k_0 (see Figure 8). As has been observed for other reactions involving the OH radical (Jiménez et al. 2015, 2016; Antiñolo et al. 2016), a downward curvature in the bimolecular plots is seen at high concentrations, probably due to dimer formation that reduces the monomer concentration. The concentration of H_2CO was always kept low enough to avoid dimerization in the timescale of the experiment. The concentration range where Equation (12) is accomplished varies with temperature, as shown in Figure 8. The temperature dependence of the obtained rate coefficients for the OH + H_2CO reaction between 22 and 107 K is displayed in Figure 9 together with literature values between 202 and 399 K from Sivakumaran et al. (2003). The

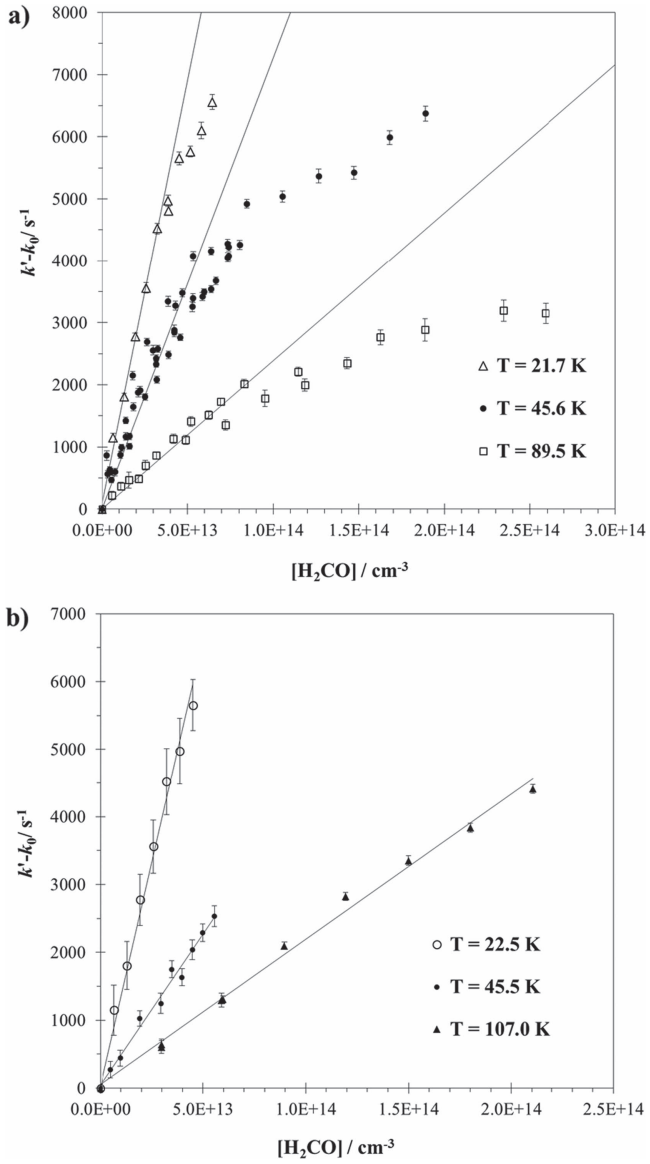

Figure 8. Pseudo–first-order plots for the OH + H_2CO reaction. (a) Example of the observed downward curvature at 21.7, 45.6, and 89.5 K. (b) Examples at 22.5, 45.5, and 107.0 K.

fitting of both data sets yields the equation presented in the figure. The confidence bands are also displayed as dashed lines.

ORCID iDs

A. Canosa https://orcid.org/0000-0001-5719-9899
M. Agúndez https://orcid.org/0000-0003-3248-3564
J. Cernicharo https://orcid.org/0000-0002-3518-2524
O. Roncero https://orcid.org/0000-0002-8871-4846

References

Agúndez, M., Cernicharo, J., & Guélin, M. 2015, A&A, 577, L5
Agúndez, M., & Wakelam, V. 2013, ChRv, 113, 8710
Akbar Ali, M., & Barker, J. R. 2015, JPCA, 119, 7578
Alvarez-Idaboy, J. R., Mora-Diez, N., Boyd, R. J., & Vivier-Bunge, A. 2001, JAChS, 123, 2018
Antiñolo, M., Agúndez, M., Jiménez, E., et al. 2016, ApJ, 823, 25
Atkinson, R., Baulch, D. L., Cox, R. A., et al. 2004, ACP, 4, 1461
Atkinson, R., Baulch, D. L., Cox, R. A., et al. 2006, ACP, 6, 3625

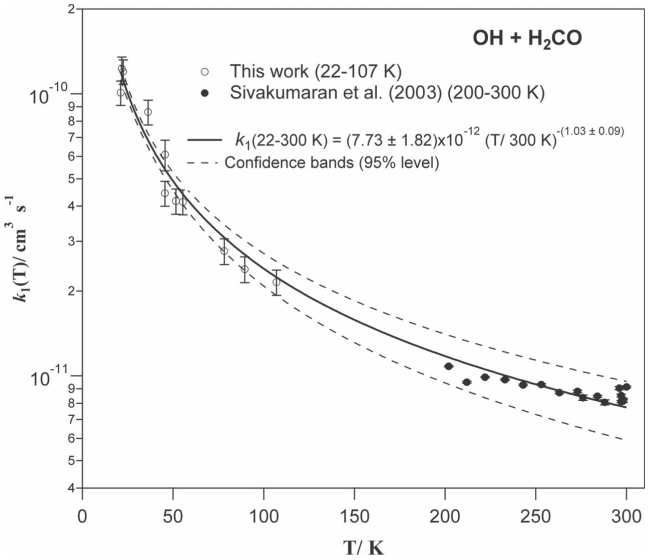

Figure 9. Temperature dependence of the rate coefficient for the OH + H_2CO reaction between 22 and 300 K.

Bacmann, A., & Faure, A. 2016, A&A, 587, A130
Bacmann, A., Lefloch, B., Ceccarelli, C., et al. 2003, ApJL, 585, L55
Böhland, T., Temps, F., & Wagner, H. G. 1984, BBGPC, 88, 455
Canosa, A., Ocaña, A. J., Antiñolo, M., et al. 2016, ExFl, 57, 152
Cernicharo, J., Marcelino, N., Roueff, E., et al. 2012, ApJL, 759, L43
Croft, J. F. E., & Bohn, J. L. 2014, PhRvA, 89, 12714
D'Anna, B., Bakken, V., Beukes, J. A., et al. 2003, PCCP, 5, 1790
Dorta-Urra, A., Zanchet, A., Roncero, O., & Aguado, A. 2015, JChPh, 142, 154301
Garrod, R. T., & Herbst, E. 2006, A&A, 457, 927
Garrod, R. T., Weaver, S. L. W., & Herbst, E. 2008, ApJ, 682, 283
Gerin, M., Goicoechea, J. R., Pety, J., & Hily-Blant, P. 2009, A&A, 494, 977
Gómez-Carrasco, S., González-Sánchez, L., Aguado, A., et al. 2004a, CPL, 383, 25
Gómez-Carrasco, S., González-Sánchez, L., Aguado, A., et al. 2004b, JChPh, 121, 4605
Gómez-Carrasco, S., Roncero, O., González-Sánchez, L., et al. 2005, JChPh, 123, 114310
Grozdanov, T. P., & Sovolev, E. A. 1982, JPhB, 15, 1195
Guzmán, V., Pety, J., Goicoechea, J. R., Gerin, M., & Roueff, E. 2011, A&A, 534, 1
Hamberg, M., Geppert, W. D., Thomas, R. D., et al. 2007, MolPh, 105, 899
Jiménez, E., Antiñolo, M., Ballesteros, B., Canosa, A., & Albaladejo, J. 2016, PCCP, 18, 2183
Jiménez, E., Ballesteros, B., Canosa, A., et al. 2015, RScI, 86, 45108
Jiménez, E., Lanza, B., Garzón, A., Ballesteros, B., & Albaladejo, J. 2005, JPCA, 109, 10903
Jiménez-Serra, I., Martín-Pintado, J., Rodríguez-Franco, A., & Marcelino, N. 2004, ApJL, 603, L49
Johnson, B. R. 1987, JChPh, 86, 1445
Karplus, M., Porter, R. N., & Sharma, R. D. 1965, JChPh, 43, 3259
Leurini, S., Parise, B., Schilke, P., Pety, J., & Rolffs, R. 2010, A&A, 511, A82
Levine, R., & Bernstein, R. B. 2001, Molecular Reaction Dynamics (Oxford: Oxford Univ. Press)
Liszt, H. S., Lucas, R., & Pety, J. 2006, A&A, 448, 253
Lourderaj, U., Park, K., & Hase, W. L. 2008, IRPC, 27, 361
Marcelino, N., Cernicharo, J., & Roueff, E. 2005, ApJ, 620, 308
Maret, S., Ceccarelli, C., Caux, E., et al. 2004, A&A, 416, 577
McElroy, D., Walsh, C., Markwick, A. J., et al. 2013, A&A, 550, A36
Nyman, G., Nordholm, S., & Schranz, H. W. 1990, JChPh, 93, 6767
Qu, C., & Bowman, J. M. 2016, JPCA, 120, 4988
Scott, G. B. I., Milligan, D. B., Fairley, D. A., Freeman, C. G., & McEwan, M. J. 2000, JChPh, 112, 4959
Shampine, L. F., & Gordon, M. K. 1975 Computer Solution of Ordinary Differential Equations: The Initial Value Problem (Albuquerque, NM: W.H. Freeman & Co)
Shannon, R. J., Blitz, M. A., Goddard, A., & Heard, D. E. 2013, NatCh, 5, 745
Shannon, R. J., Taylor, S., Goddard, A., Blitz, M. A., & Heard, D. E. 2010, PCCP, 12, 13511

Siebrand, W., Smedarchina, Z., Martínez-Núñez, E., & Fernández-Ramos, A. 2016, PCCP, 18, 22712
Sivakumaran, V., Hölscher, D., Dillon, T. J., et al. 2003, PCCP, 5, 4821
Snyder, L. E., Buhl, D., Zuckerman, B., & Palmer, P. 1969, PhRvL, 22, 679
Tafalla, M., Myers, P. C., Mardones, D., & Bachiller, R. 2000, A&A, 359, 1
Wakelam, V., Loison, J.-C., Herbst, E., et al. 2015, ApJS, 217, 20
Wang, S., Davidson, D. F., & Hanson, R. K. 2015, Proc Combust Inst, 35, 473
Woods, P. M., Slater, B., Raza, Z., et al. 2013, ApJ, 777, 90
Xu, S., Zhu, R. S., & Lin, M. C. 2006, Int J Chem Kinet, 38, 322
Young, K. E., Lee, J., Evans, N. J., II, Goldsmith, P. F., & Doty, S. D. 2004, ApJ, 614, 252
Zanchet, A., Del Mazo, P., Aguado, A., et al. 2017, PCCP, in press, doi:10.1039/c7cp05307J
Zhang, W., Du, B., & Qin, Z. 2014, JPCA, 118, 4797
Zhao, Y., Wang, B., Li, H., & Wang, L. 2007, JMoSt, 818, 155